이학석사 학위논문

Photo-crosslinked polymer cubosomes as a recyclable nanoreactor in organic solvents

유기 용매에서 재활용 가능한 나노반응기로서의 광-가교 되어진 고분자 큐보좀에 대한 연구

2021 년 8 월

서울대학교 대학원

화학부 고분자화학 전공

권 준 호

Photo-crosslinked polymer cubosomes as a recyclable nanoreactor in organic solvents

지도 교수 김 경 택

이 논문을 이학석사 학위논문으로 제출함
2021 년 08 월

서울대학교 대학원
화학부 고분자 전공
권 준 호

권준호의 이학석사 학위논문을 인준함
202 1년 08 월

위 원 장 **손 병 혁**

부위원장 **김 경 택**

위 원 **최 태 림**

ABSTRACT

Photo-crosslinked polymer cubosomes as a recyclable nanoreactor in organic solvents

Jun Ho Kwon

Polymer Chemistry in Department of Chemistry

The Graduate School

Seoul National University

Polymer cubosomes are an emerging class of mesoporous structures formed by the solution self-assembly of block copolymers (BCPs) with a highly asymmetric block ratio. The internal nanochannel networks of a polymer cubosome provide a large surface area and internal volume to accommodate catalysts, which makes this reticulated porous structure a promising candidate for nanoreactors. Herein, we report the synthesis of BCPs composed of poly(ethylene glycol) (PEG) hydrophilic and poly(styrene-*co*-pentafluorostyrene) (P(pFS-*co*-Sty)) hydrophobic block. The pentafluorophenyl groups in the hydrophobic block could be easily functionalized with N_3 groups by post-polymerization modification. The binary mixture of branched-linear and catalyst-functionalized linear BCP self-assembled into polymer cubosomes having surface-tethered catalysts, which was crosslinked by

UV irradiation. We show that the resulting polymersome nanoreactors could catalyze the asymmetric aldol reaction of 4-nitrobenzaldehyde and acetone in organic solvents to yield (R)-4-hydroxy-4-(4-nitrophenyl)butan-2-one at an enhanced rate compared to the reaction catalyzed by molecular catalysts. These robust nanoreactors performed the catalysis repeatedly after multiple recycling without losing their catalytic efficiency and structural integrity.

Keywords : block copolymer, photo-crosslinking, organo-catalytic reaction, solution self-assembly, cubosome

Student Number : 2019-27820

Table of Contents

List of Figures, Schemes, and Tables

Figures

Schemes

Tables

I. INTRODUCTION

Nanoreactors enhance the rate and selectivity of the reaction by confining the catalysts within the porous cage allowing diffusion of reagents and products.[1-3] The confinement also protects the degradation of catalysts, which enables the nanoreactors to be recycled by utilizing the size difference of nanoreactors compared to the reagents and products. Polymer platform such as micelles, star polymers and polymersome have been utilized as nanoreactors for biological and chemical transformation by making the compartmentalizing membrane permeable.[4-11] Polymer cubosomes (PCs)[12-15] are an emerging class of mesoporous structures formed by the solution self-assembly of block copolymers (BCPs) with a highly asymmetric block ratio[16-18] into inverse mesophases. PCs are composed of triply periodic minimal surfaces (TPMSs) of BCP bilayers,[19,20] in which two reticulated nanochannel networks are embedded in the internal cubic crystalline membrane surrounded by a perforated bilayer crust.[21] Guest molecules can diffuse into the internal nanochannel networks of a PC through the perforated surface, exposing the organized nanoconfinement to the surroundings.[22-25] In addition, PCs provide a large and well defined internal surface area for anchoring functional groups compared with other polymer based catalysis platform.[13,26] These structural characteristics make these PCs a unique nanoreactor for conducting chemical and biochemical reactions by allowing free access of the guest molecules, ranging from small molecules to proteins,[15] to the surface-tethered catalysts[27,28] or enzymes[13] on the surface of the inner compartment of polymer cubosome.

Lipid cubosomes[29–32] share the same structural characteristics with polymeric counterparts and have been used as nanoreactors by covalently anchoring catalysts on the internal TPMS of lipid bilayers.[19,33] In a similar manner, PCs also have been utilized as bioreactors performing reactions catalyzed by covalently anchored

enzymes.[13] However, unlike biochemical substrates, most chemical transformations are conducted in organic solvents. To utilize these PCs as nanoreactors that provide the confinement required for chemical reactions conducted in organic solvents, the structural integrity of PCs must be maintained in organic solvents. The transient nanostructures formed by the self-assembly of the BCPs can be stabilized by covalent crosslinking between the BCPs.[34-38]

Herein, we report a crosslinked PC as a robust nanoreactor that can be utilized for chemical transformations in an organic solvent. The complex inner structure of the PC can be retained by photo-crosslinking the hydrophobic domain of the BCP bilayers composing the TPMS.[39,40] The photo-crosslinkable BCPs were prepared by atom transfer radical copolymerization (ATRP) of styrene (Sty) and 2,3,4,5,6-pentafluorostyrene (pFS) in the presence of poly(ethylene glycol) macroinitiators. The post-polymerization modification on pentafluorophenyl groups of the BCPs introduced photodegradable azide groups into the poly(pentafluorophenyl-co-styrene) (P(pFS-*co*-Sty)) hydrophobic block.[41] The PCs formed by the self-assembly of BCP containing the hydrophobic P(pFS-*co*-Sty) block with azide groups were covalently stabilized without morphological changes in aqueous solutions upon irradiation with UV light. The crosslinked PCs retained their structural integrity in common organic solvents such as THF. The large surface area of the PCs allowed them to be utilized as an efficient platform for conducting the asymmetric aldol reaction in organic solvents (Fig. 1). The polymersome nanoreactors could also be recycled for conducting multiple reactions without losing their catalytic ability.

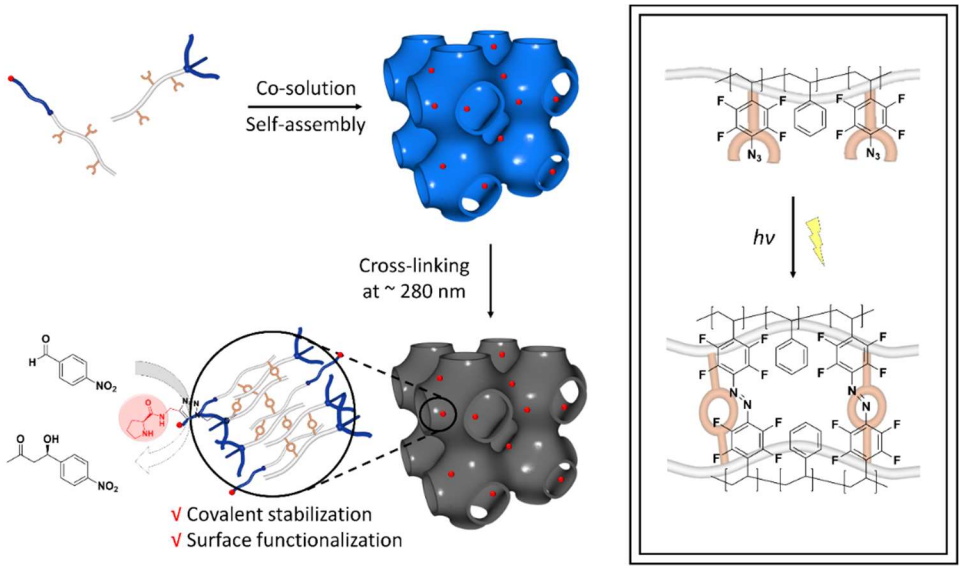

Fig. 1 Schematic representation of a branched-linear BCP having poly(styrene-*co*-2,3,5,6-fluoro-4-azido-styrene) (P(pFS-*co*-Sty)) as a hydrophobic block and its self-assembly into complex inverse bicontinuous bilayers. From the solution self-assembly of the branched-linear BCP, the polymer cubosomes (PCs) having internal primitive cubic minimal surface (*Im*3*m*) was formed. After photo-crosslinking of the hydrophobic P(pFS-*co*-Sty) blocks, the covalently stabilized PCs retain their large surface and can be used as an efficient platform for conducting the asymmetric aldol reaction in an organic solvent.

II. RESULTS AND DISCUSSION

Synthesis of photo-crosslinkable block copolymers.

Well-defined poly(2,3,4,5,6-pentaflurostyrene) (PpFS) has recently drawn significant attention due to the post-polymerization modification of the pentafluorophenyl pendants via nucleophilic aromatic thiol–para-fluoro substitution[42] or azide–para-fluoro substitution.[41,43] These fully or partially fluorinated polymers have been synthesized by controlled radical

polymerization[44,45] and anionic polymerization.[46] Under the radical polymerization conditions, P(pFS-*co*-Sty) favors to have microstructures consisting of alternating sequences of pFS and Sty.[47] Recently, Wu and coworkers have synthesized partially fluorinated polymers by the alternating copolymerization of pFS and Sty via reversible addition-fragmentation chain transfer (RAFT) polymerization.[48] We adopted an atom-transfer radical polymerization (ATRP) in anisole to prepare random copolymers of pFS and Sty as the PpFS homopolymer is insoluble or sparingly soluble in common organic solvents such as THF and chloroform. Despite a strong tendency to form alternating copolymers by ATRP, the copolymerization of Sty and pFS in aromatic solvent with high temperature prefers to form random copolymers.[47,49] First, we synthesized a BCP with an equal amount of monomers (pFS:Sty = 5:5 mol/mol) by using branched PEG macroinitiator (Fig. 2A). The molecular weight of the BCP increased linearly with the polymerization time without the deterioration of the molecular weight distribution up to 70% conversion. The resulting **BCP1** was fully characterized by ^{1}H and ^{19}F nuclear magnetic resonance (NMR) spectroscopy and gel permeation chromatography (GPC) (Fig. 8, 10 and 11) The random sequence of pFS and Sty in the hydrophobic block was corroborated by ^{1}H-^{13}C heteronuclear multiple bond correlation (HMBC) experiment. The ^{13}C NMR projection of the HMBC spectrum showed the peaks corresponding three possible types of styrene-centered monomer triads, Sty-*Sty*-Sty (40.8 ppm), pFS-*Sty*-Sty (42 ppm), and pFS-*Sty*-pFS (42.8 ppm). The presence of the HMBC peaks corresponding the Sty-*Sty*-Sty triad with pFS-*Sty*-Sty and pFS-*Sty*-pFS triads suggested the randomized sequence of monomers along the hydrophobic block (Fig. 2B and Fig. 12).[50]

In order to maximize the number of pFS units in the hydrophobic block, we synthesized **BCP2** with a monomer mixture containing 70% of pFS (pFS:Sty =

7:3 mol/mol) under the same condition used for the ATRP of **BCP1**. The ^{1}H and ^{13}C NMR analysis of **BCP2** showed an increased composition of pFS in the hydrophobic block, which coincided with the feed ratio of pFS (Fig. 9). The monomer mixture containing over 70% of pFS did not result in the formation of well-defined copolymers by the ATRP.

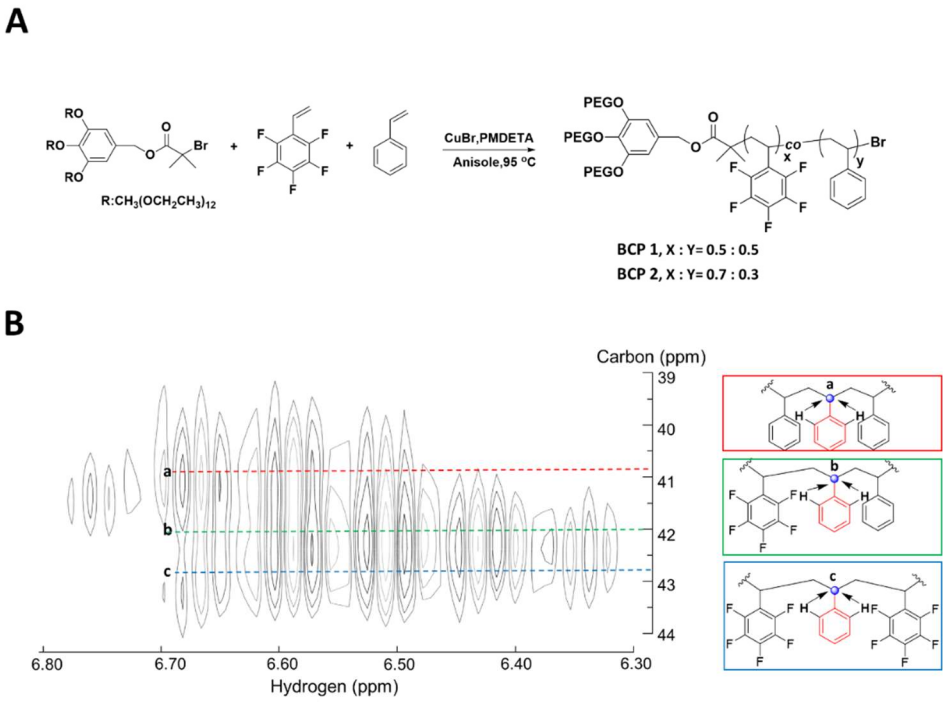

Fig. 2 (A) Synthesis of PEG-P(pFS-*co*-Sty) block copolymers composed of branched hydrophilic PEG blocks and random copolymer of pFS and PS as hydrophobic blocks. (B) Enlarged image of NMR spectra in red circle and ^{13}C NMR projection showing peaks corresponding three types of styrene-centered monomer triads. Entire image of ^{1}H-^{13}C heteronuclear multiple bond correlation (HMBC) data is in Fig. 12.

Table 1. Characterization of the prepared block copolymers.

Sample	Initiator	DP$_n$ (Sty)[a]	DP$_n$ (pFS)[a]	f_{PEG} (%)[b]	M_n (kg mol^{-1})[c] of BCPs	M_w (kg mol^{-1})[c] of BCPs	$Đ$[c] of BCPs
BCP1	$(PEG550)_3$	115	115	4.8	22.2	25.4	1.14
BCP2	$(PEG550)_3$	79	185	4.5	21.8	25.8	1.18
L1	TMS-ABIB[d]	132	132	5.1[e]	19.5	22.5	1.15

[a]Degree of polymerization (DP_n) calculated with ^{1}H-NMR. [b]Molecular weight ratio of the PEG domain (f_{PEG}) to the hydrophobic block (1650 g mol^{-1} for $(PEG550)_3$ initiators). [c]Number average molecular weight (M_n) and molecular weight distribution ($Đ$) determined by GPC using polystyrene (PS) standards. [d]3-(trimethylsilyl)prop-2-yn-1-yl 2-bromo-2-methylpropanoate. [e]Calculated after the connection between (PEG2000).

Self-assembly of BCPs in dilute solution.

We synthesized **BCP1** and **BCP2** to possess an identical block ratio and overall molecular weight for their preferential self-assembly into PCs in dilute solution (Table 1). **BCP1** was allowed to self-assemble from the dioxane solution (1 wt%) by introducing an equal volume of water for 4 h, followed by dialysis against water. The self-assembly of **BCP1** to PCs was confirmed by transmission electron microscopy (TEM) and scanning electron microscopy (SEM). The fast Fourier Transformation (FFT) analysis of the TEM images (Fig. 3A) suggested that the internal TPMS of the PCs of **BCP1** was composed of Schwarz P surface (*Im*3*m* space group).[51] This assessment was confirmed by the small angle X-ray scattering (SAXS) results obtained from dried PCs of **BCP1** (*Im*3*m* space group, lattice parameter (a) = 69.3 nm) (Fig. 3C).

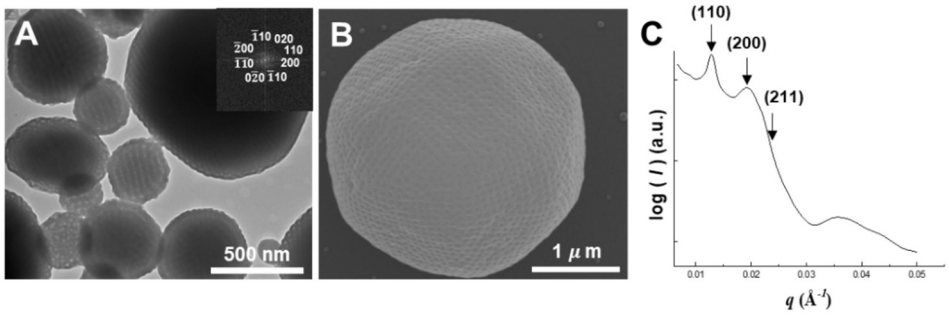

Fig. 3 (A) Representative TEM image of polymer cubosomes of **BCP1** with the fast Fourier transform (FFT) images shown in the inset. Cubosomes in the TEM image were viewed along the [100] direction. (B) SEM image and (C) SAXS analysis of the self-assembled structure showing inner structure of PC was composed of Schwarz P surface (*Im*3*m* space group, lattice parameter (*a*) = 69.3 nm).

We investigated the effect of the composition of pFS in the hydrophobic block on the self-assembly of the BCP in dilute solution. The electron microscopy (EM) study of the self-assembled structures of **BCP2** built with the hydrophobic block containing 70% of pFS units in the backbone mostly showed polymer vesicles along with a small number of disordered bicontinuous colloidal particles (sponge-phase particles). To optimize the conditions for the formation of PCs of **BCP2**, we screened the conditions affecting the self-assembly such as common solvents, the concentration of the BCP in solution, and the rate of water addition. Interestingly, the self-assembly of **BCP2** showed a strong dependency on the rate of water addition to the dioxane solution of the BCP. When the time of water addition was reduced from 4 h to 0.5 h, **BCP2** self-assembled to spherical sponge-phase particles having a dense core, resembling a cell with a nucleus (Fig. 4A and 4B). When the water addition time was further slowed down to 1 h, the sponge-phase particles transformed to axially stretched particles reminiscent of fibroblast. The internal structures of these particles consisted of disordered bicontinuous phases of BCP bilayers (Fig. 4C and 4D). Essentially, fibroblast-shaped particles dissociated to polymer vesicles upon further slow-down of the water addition (4 h). This observation suggested that the fibroblast-like bicontinuous particles might be an intermediate in the evolution of sponge-phase particles to polymer vesicles. In contrast to the morphological transformation of the aggregates of **BCP2** upon

increasing the time allowed for self-assembly, the self-assembly of **BCP1** did not show any dependency on the change of the time of water addition, which only showed the formation of PCs regardless of the time for water addition. (Fig. 15). We suspect that this difference in the self-assembly behavior of BCPs could be attributed to the increased composition of pFS unit in the hydrophobic block for **BCP2**, causing the instability of the hydrophilic block at a low water content in the solution due to the reduced solubility of the pFS unit compared to the solubility of styrene.

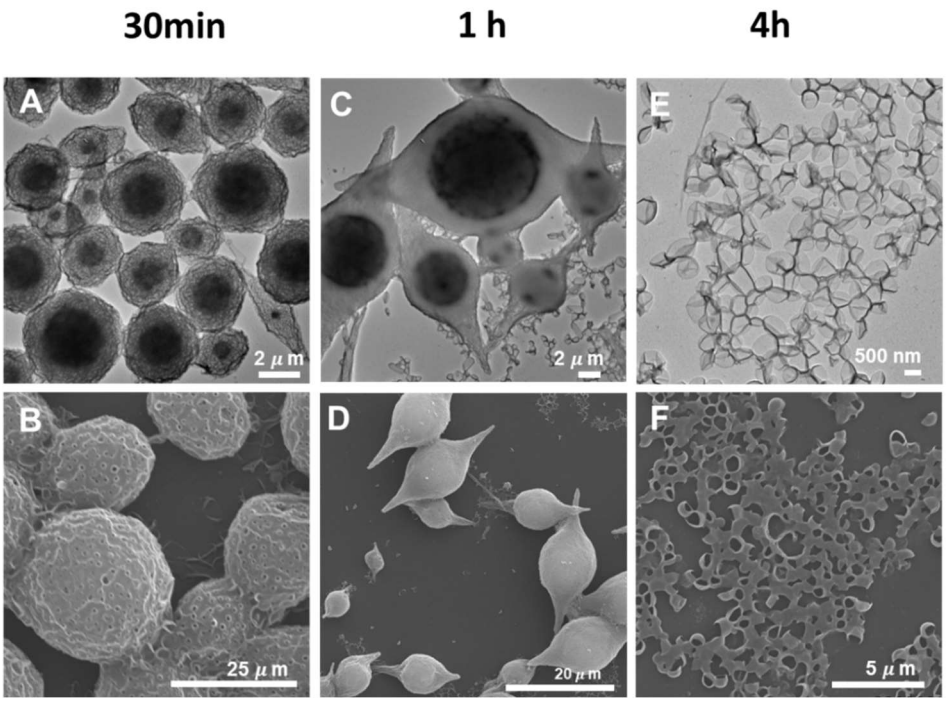

Fig. 4 (A, C and E) TEM and (B, D and F) SEM images of the self-assembled structures of **BCP2** as a function of the water-injection time: (Time of water addition (t) = 30 min for A and B) spherical sponge-phase particles with dense core; (t = 1 h for C and D) fibroblast shaped sponge-phase particles; and (t = 4 h for E and F) polymer vesicles. Inner structure of B and D are in SI in Fig. 19.

Post-polymerization modification of BCPs for photo-crosslinking of PCs.

Pentafluorophenyl pendant groups in P(pFS-*co*-Sty) block of **BCP1** can be readily functionalized at *p*-position of pentaflurorophenyl unit by the post-polymerization modification of the BCP with NaN_3 in DMF, resulting in the BCP having *p*-azido-tetrafluorophenyl groups (**BCP1**-N_3).[39] ^{19}F NMR of **BCP1** after the modification showed that 56.4% of pFS units were converted to *p*-N_3-TFS (Fig. 5A). The presence of the azide groups on the P(pFS-*co*-Sty) was also confirmed by Fourier-transform infrared(FT-IR) spectroscopy showing the strong N≡N stretching band at 2125 cm^{-1}. (Fig. 5B). After azide substitution, we checked thermal properties of P(pFS-*co*-Sty)-N_3 with Thermo Gravimetric Analysis (TGA) and Differential Scanning Calorimetry (DSC) (Fig. 13C). As a result, this azide-containing polymer should be handled under 100 °C to suppress explosive degradation of azide group and protected with silver foil to avoid photo-degradation.

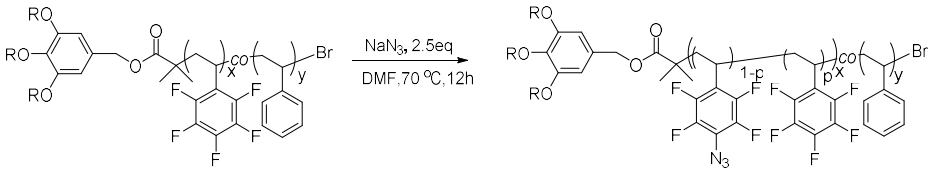

Scheme 1. Post-polymerization azide modification of **BCP1**.

BCP1-N_3 self-assembled into PCs having the internal Schwarz P surface (*Im*3*m* space group) which was identical to the lattice symmetry of the PCs of **BCP1** (Fig. 5C). The well-defined periodic minimal surface was analyzed by FFT

analysis with electron microscopy and small angle x-ray scattering (SAXS) (*Im*3*m* space group, a = 61.2 nm). (Fig. 5D). To covalently stabilize the PCs of **BCP1**-N_3, the dispersion was irradiated with UV light irradiation (λ = ~280 nm, 20 W) for 8 h. After irradiation, the medium of the dispersion was exchanged from water to THF by dialysis. We investigated the internal order of the crosslinked PCs of **BCP1**-N_3 dispersed in THF for 24 h. The EM images and the SAXS result of the dried PCs evidenced that the structural integrity of the PCs was maintained without change. The lattice constant of the internal Schwarz P surface of the PCs was decreased from 61.2 nm of the pristine cubosomes of **BCP1**-N_3 to 60.5 nm of the crosslinked ones. The EM images also confirmed that the pore size of the surface and the diameter of the internal channel networks were preserved without significant changes. (Fig. 5E and 5F). Without the irradiation, the polymersomes of **BCP1**-N_3 completely dissolved to the corresponding BCP after the solvent exchange from water to THF.

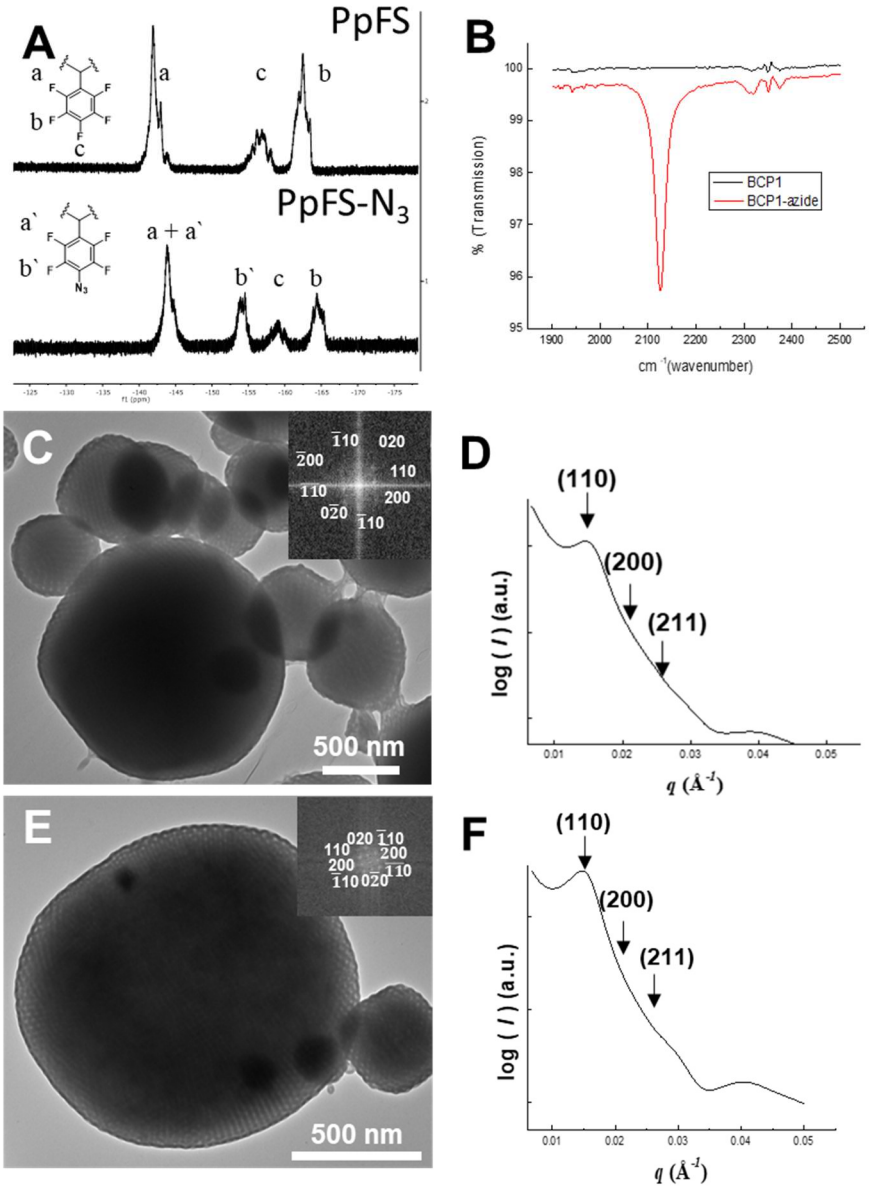

Fig. 5 (A) ^{19}F NMR and (B) Fourier-transform infrared (FT-IR) spectra of **BCP1** and **BCP1**-N_3. FFT analysis with TEM images on [100] direction and SAXS curve of the PCs of **BCP1**-N_3 showing primitive cubic structure (*Im*3*m* space group) (C and D) before and (E and F) after photo-crosslinking.

Crosslinked PC nanoreactor with surface-tethered L-proline.

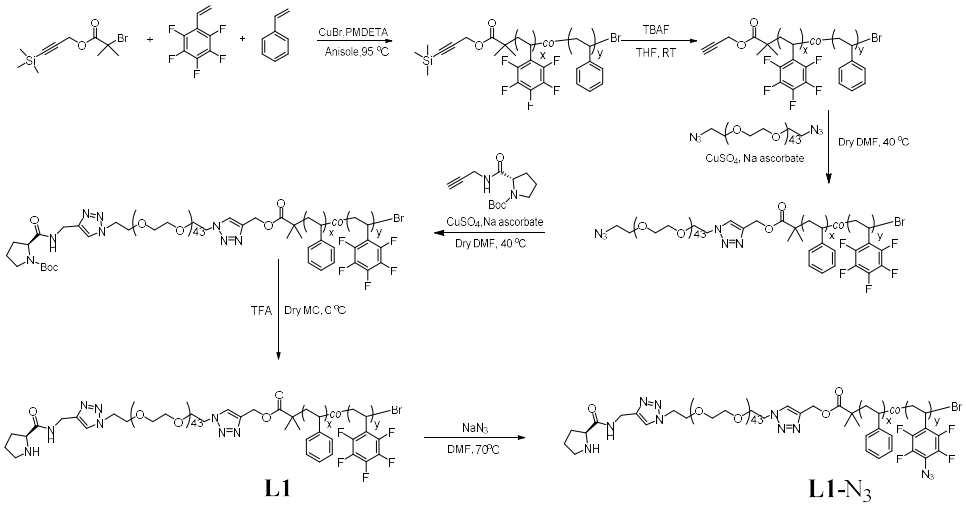

Scheme 2. Synthesis of linear telechelic proline (PEG2000)-*b*-P(pFS-*co*-Sty).

The internal nanochannel networks are exposed to the surroundings through the porous crust of the PCs, allowing the diffusion of reagents to reach the catalysts anchored on the internal minimal surface. Therefore, we constructed cubosome-based nanoreactors by implementing organocatalytic L-proline moieties to the self-assembled BCP bilayers composing the PCs. For the implementation, we co-assembled the BCP blend of **BCP1**-N_3 and a linear BCP having L-proline at the PEG end, **L1**-N_3, (9:1 w/w) to form PCs by the same self-assembly method.[26] The PCs of the BCP blend of **BCP1**-N_3 and **L1**-N_3 (9:1 w/w) was examined by SEM (Fig. 6B and 6C) and TEM (Fig. 6D and 6E), which confirmed that the resulting PCs possessed well-defined internal TPMS with a long range cubic crystalline order. The SEM images showed the surface pores remained on the outermost crust of the PCs and the internal reticulated channel networks were open

to the surroundings. The resulting PCs were photo-crosslinked by irradiating UV light (~ 280 nm) for 8 h.

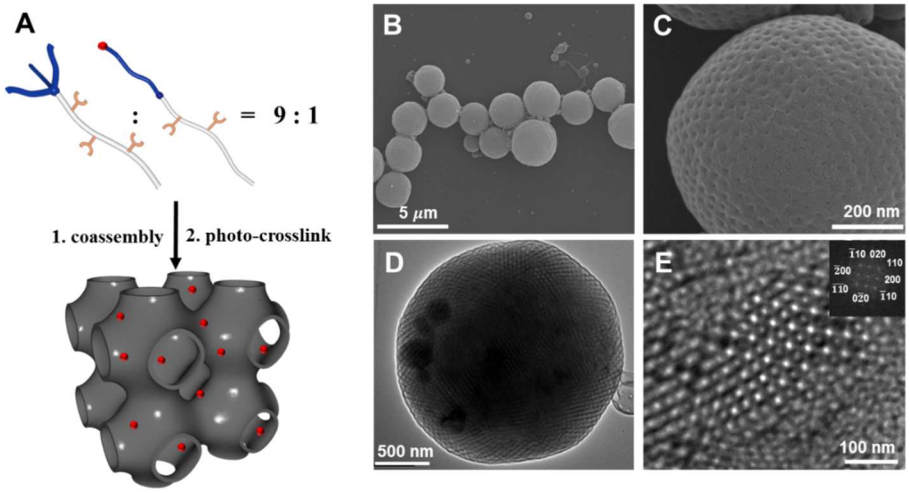

Fig. 6 (A) Schematic representation of the coassembly of **BCP1**- N_3 and **L1**- N_3 with (9:1) ratio. (B and C) SEM and (D and E) FFT analysis of HR-TEM images on [100] direction of the crosslinked polymer cubosomes showing spherical shape, porous morphology, and high crystalline inner structure with *Im*3*m* space group.

The PC nanoreactors would expose long PEG chains having L-proline at the chain end protruding from the internal TPMS. The surface-tethered organocatalysts residing in the nanochannel networks would catalyze the reaction of the reagents diffused in the nanochannel networks through the surface pores of the PC nanoreactors. To examine the catalytic activity of the crosslinked PC nanoreactors in an organic solvent, we performed asymmetric aldol reaction of 4-nitrobenzaldehyde and acetone to yield (*R*)-4-hydroxy-4-(4-nitrophenyl) butan-2-one in THF. The reaction was carried out by adding the photo-crosslinked PC

nanoreactors with surface-tethered proline (50 mg) in the THF solution of the equimolar mixture of 4-nitrobenzaldehyde and acetone, followed by shaking the solution at room temperature. The progress of the reaction was monitored by ^{1}H NMR (Fig. 7A), which indicated the completion of the reaction in 72 h with an enantiomeric excess (ee) of 44% determined by chiral stationary high-performance liquid chromatography (Fig. 22). Next, we compared the conversion over the reaction time of the same reaction catalyzed by the PC nanoreactor and homogeneous L-proline. The concentration of L-proline tethered to the PC nanoreactor (50 mg 2 mL^{-1}) was calculated by assuming the full exposure of the PEG-attached L-proline (2.42 μmol g^{-1}) (for calculation, see the SI) on the TPMS of the PC of the BCP having ~80 m^2 g^{-1} of surface area.[26] The conversion of the aldol reaction catalyzed by homogeneous catalyst (0.26 μmol) reached 80 % after 100h. With the same concentration of the organocatalyst, the PC nanoreactor only required 36 h to achieve the same conversion (Fig. 7B and 7C). This result showed that the crosslinked PC nanoreactors perform the catalysis at an enhanced reaction rate to that of the aldol reaction carried out with a molecular catalyst. In addition, the surface-tethered L-proline catalyzed the reaction without significant losing of the stereochemical selectivity compared with homogeneous state L-proline catalysis.[52-53]

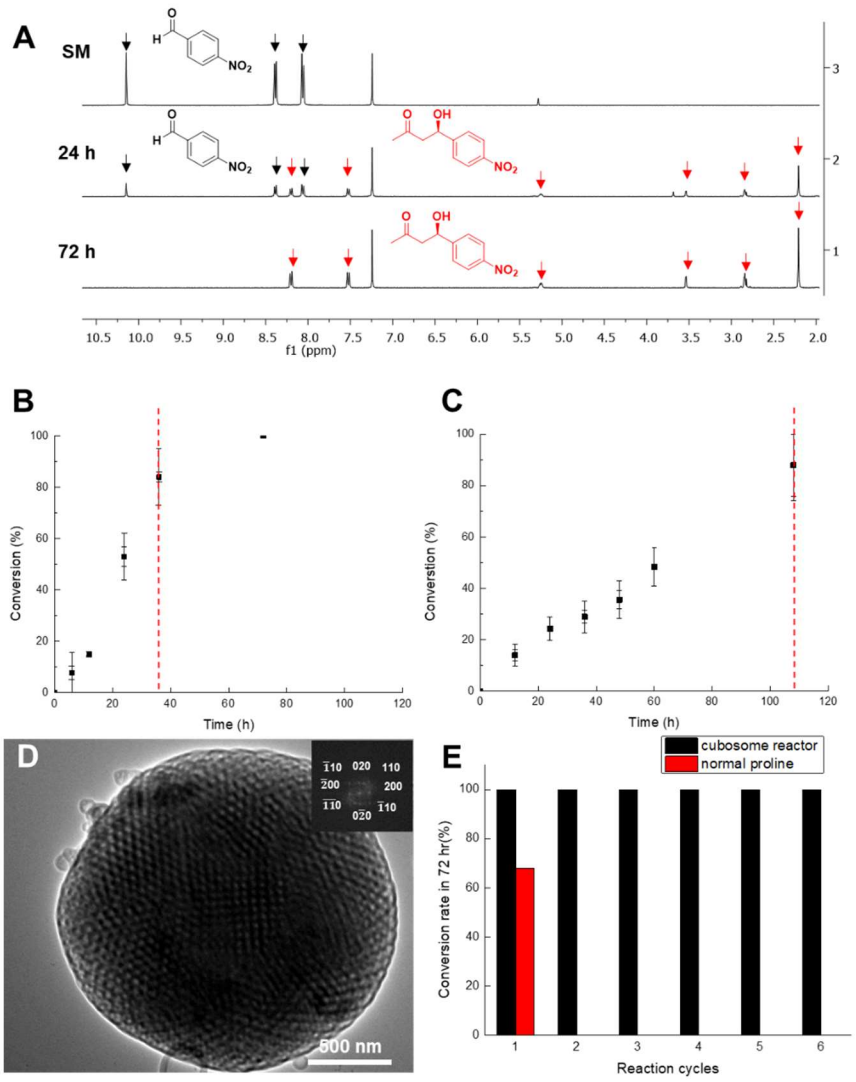

Fig. 7 (A) Conversion rates of the model aldol reaction of 4-nitrobenzaldehyde and acetone in the cubosome-based nanoreactor from the ^{1}H NMR spectra at 0 h, 24 h, and 72 h. Conversion rate of the aldol reaction with (B) proline-functionalized PCs and (C) homogeneous L-proline. (D) HR-TEM image of **BCP1**-N_3/**L1**-N_3 (9:1) coassemble PC after aldol reactions, indicating the preservation of the reactive surface with FFT analysis on [100] direction. (E) Reusability test of the cubosome nanoreactor compared with homogeneous state L-proline in organic solvent for the asymmetric aldol reaction in 72 hours.

After the completion of the reaction, the PC nanoreactors were recollected by centrifugating the reaction mixture on a centrifugal filter, followed by washing with THF. The collected PC nanoreactors were examined by FFT analysis with TEM on [100] direction, which showed no structural degradation on the surface and the retention of their inner primitive cubic structure after the 72 h in a reaction condition. (Fig. 7D) We tested the recyclability of the crosslinked PC nanoreactor by repeating the asymmetric aldol reaction by redispersing the collected PC nanoreactor in the reaction mixture. The crosslinked PC nanoreactor showed the complete conversion of reagents in 72 h (Fig. 7E) up to six recycling steps. These results suggested that the crosslinked PC nanoreactors could catalyze the chemical reactions in organic solvents in a recyclable manner without suffering the loss of reactivity caused by the deterioration of nanostructural details of the PC.

III. CONCLUSION

In summary, we synthesized photo-crosslinkable BCPs by introducing pentafluorostyrne (pFS) units in the hydrophobic block. The atom-transfer radical copolymerization of styrene and pFS in the presence of linear or branched PEG macroinitiators yielded well-defined BCPs having P(pFS-*co*-Sty) hydrophobic blocks, which subsequently functionalized with azide groups by post-polymerization modification of BCPs. The co-assembly of the PC-forming BCP and the linear BCP sharing the photo-crosslinkable P(pFS-*co*-Sty) block preferentially formed well-defined PCs in aqueous solution. The resulting PCs were photo-crosslinked under the irradiation of UV light, which converted the transient PC structures to the covalently stabilized structures maintaining the complex PC structures in organic solvents. Photo-crosslinked PCs were demonstrated as recyclable nanoreactors for aldol reaction in organic solvents, which could be performed at an enhanced rate compared to the same reaction catalyzed by molecular catalysts. Importantly, the repeated use of the recycled PC nanoreactors did not show the deterioration of the catalytic ability caused by the damage of the structural details of PC nanoreactors under repeated exposure to harsh reaction conditions. We envisage that the PC nanoreactors reported here could serve as a catalytic platform to perform a target reaction by introducing the desired catalysts to the linear BCP used for the blend for the co-assembly.

IV. Experimental Section

Materials

Unless otherwise noted, all reagents and chemicals were purchased from Sigma Aldrich, Alfa Aesar, and TCI and used as received. Styrene and 2,3,4,5,6-Pentafluorostyrene were purified by passing through a basic alumina column before polymerization. Dimethylformamide (DMF) and dichloromethane (CH_2Cl_2) were distilled over CaH_2 under N_2. Tetrahydrofuran (THF) was refluxed over a mixture of Na and benzophenone under N_2 atmosphere and distilled before use. All reactions were performed in an inert atmosphere unless otherwise noted.

General Information

^{1}H NMR, ^{13}C NMR, ^{19}F NMR and ^{1}H-^{13}C HMBC NMR spectra were recorded by Agilent 400-MR DD2 Magnetic Resonance System and Varian/Oxford As-500 using CD_2Cl_2 and $CDCl_3$ as solvents and internal standards. Molecular weights and polydispersity indices of polymers and block copolymers were measured by Agilent 1260 Infinity gel permeation chromatography (GPC) system equipped with a PL gel 5 μm MiniMIX-D column (Agilent Technologies) and differential refractive index detectors. THF was used as an eluent with a flow rate of 0.3 mL min^{-1} at 35 ˚C. A PS standard kit (Agilent Technologies) was used for calibration. Differential scanning calorimetry (DSC) was carried out under N_2 gas at a scan rate of 15 °C min^{-1} with TA Instruments Q10. Transmission electron microscopy (TEM) was performed on a Hitachi 7600 operating at 100 kV and JEOL JEM-2100 operating at 200 kV. Specimens were prepared by placing a drop of the solution on a carbon-coated Cu grid (200 mesh, EM science). After 30 min, remaining solution

on a grid was removed with a filter paper, and the grid was dried overnight. Scanning electron microscopy (SEM) was performed on a Hitachi S-4300 operating at 15 kV. Suspension was cast and dried on a slide glass, and coated with Pt by using a Hitachi E-1030 ion sputter. UV-Vis spectrometry (UV-Vis) was measured on a Jasco V-630 spectrophotometer. Synchrotron small-angle X-ray scattering (SAXS) data were obtained on the SAXS beamline (PLS-II 6D, 11.18 keV, 6.5 m) at Pohang Accelerator Laboratory. The concentrated suspension of the polymer cubosome was dried for a day in a freeze-dryer. Ti-SBA standard was used. UV light sources were Vilber VL-6.LC (254 nm/365 nm, 6 W), and Sankyo G40T10E compact UV-B lamp (output 20 W). ImageJ software (https://imagej.nih.gov/ij/) was used to conduct 2D fast Fourier transform (FFT) on TEM images. Lattice constants of polymer cubosomes were calculated from the FFT images.

Polymerization of the block copolymer containing styrene and 2,3,4,5,6-pentafluorostyrene.

All polymerizations were performed according to the same procedure. The following procedure outlines the copolymerization of styrene and 2,3,4,5,6-pentafluorostryene as an example. CuBr (22 mg, 0.15 mmol) and *N,N,N',N'',N''*-pentamethyldiethylenetriamine (PMDETA) (52 mg, 0.3 mmol) were mixed with anisole (0.5 mL) in a 15 mL Schlenk tube. A solution of 2,3,4,5,6-pentafluoro styrene (291 mg, 1.5 mmol), styrene (157 mg, 1.5 mmol) and ethyl α-bromoisobutyrate (2.9 mg, 15 μmol) in anisole (2 mL) was added to the Schlenk tube. The solution was degassed by bubbling N_2 for 15 min. After degassing, the

tube was immersed in a preheated oil bath (95 °C) and the polymerization proceeded at this temperature. The polymerization progress was monitored using Gel Permeation Chromatography (GPC) at 2 h intervals. When the molecular weight of the BCP reached the desired value, the reaction was quenched by exposing the solution to air in a liquid nitrogen with isotherm bath and diluted with $CHCl_3$ (2 mL). The quenched solution was filtered through alumina (basic, 20 mL) using $CHCl_3$ as an eluent. The filtered solution was evaporated under reduced pressure and precipitated into methanol (50 mL). The white powder was collected by vacuum filtration and dried. For BCPs, the branched poly(ethylene glycol) (PEG) macroinitiators were used for polymerization. The molecular weight and composition of the polymers were characterized by ^{1}H NMR, ^{19}F NMR and GPC.

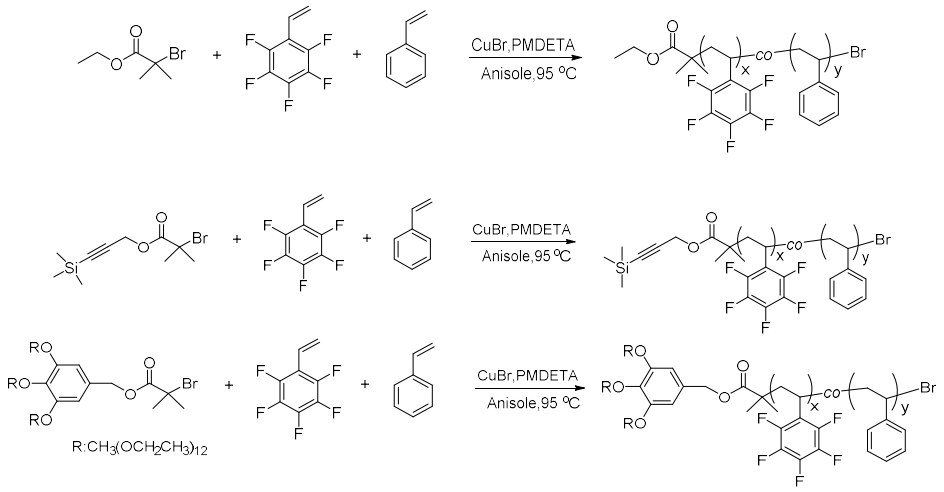

Scheme 3. Synthetic scheme of P(pFS-*co*-Sty) with different initiators.

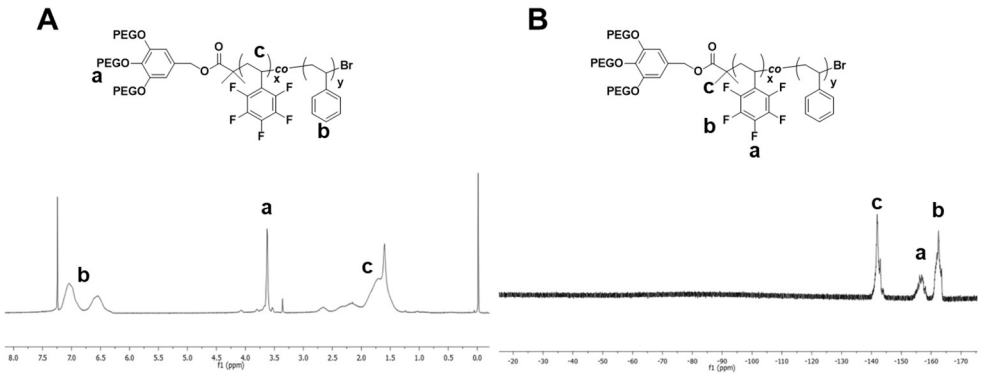

Fig. 8 ^{1}H NMR and ^{19}F NMR of $(PEG550)_3$-P(pFS-*co*-Sty) (5:5 mol/mol).

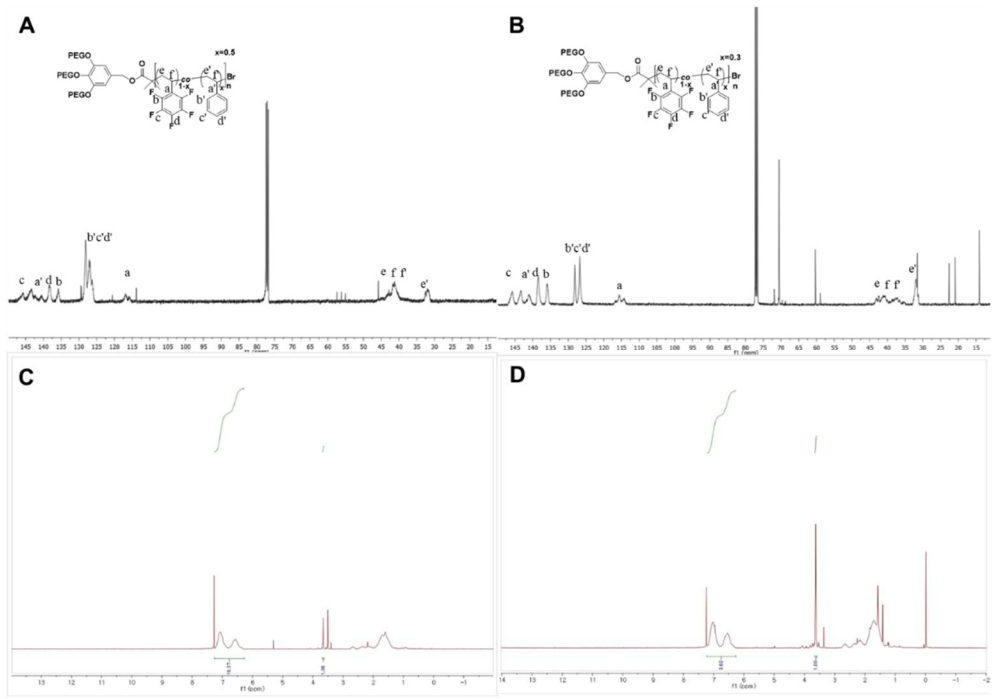

Fig. 9 ^{13}C NMR (A and B) and ^{1}H NMR (C and D) of $(PEG550)_3$-P(pFS-*co*-Sty) (5:5 mol/mol) (A and C) and $(PEG550)_3$-P(pFS-*co*-Sty) (7:3 mol/mol) (B and D).

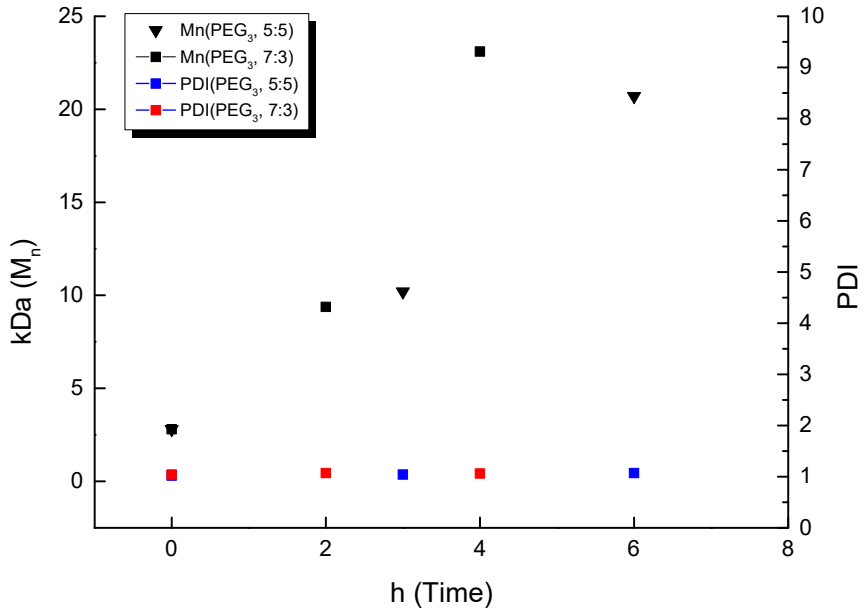

Fig. 10 Molecular weight (M_n) and molecular weight distribution (PDI) of the BCPs determined by GPC during the course of polymerization.

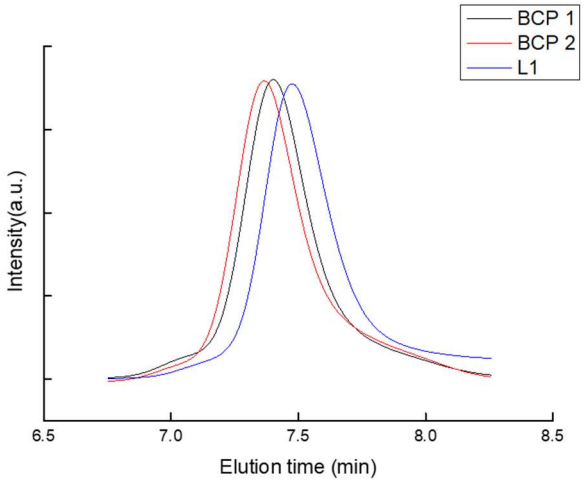

Fig. 11 GPC traces of the polymers **BCP 1** (black), **BCP 2** (red), **L1** (blue).

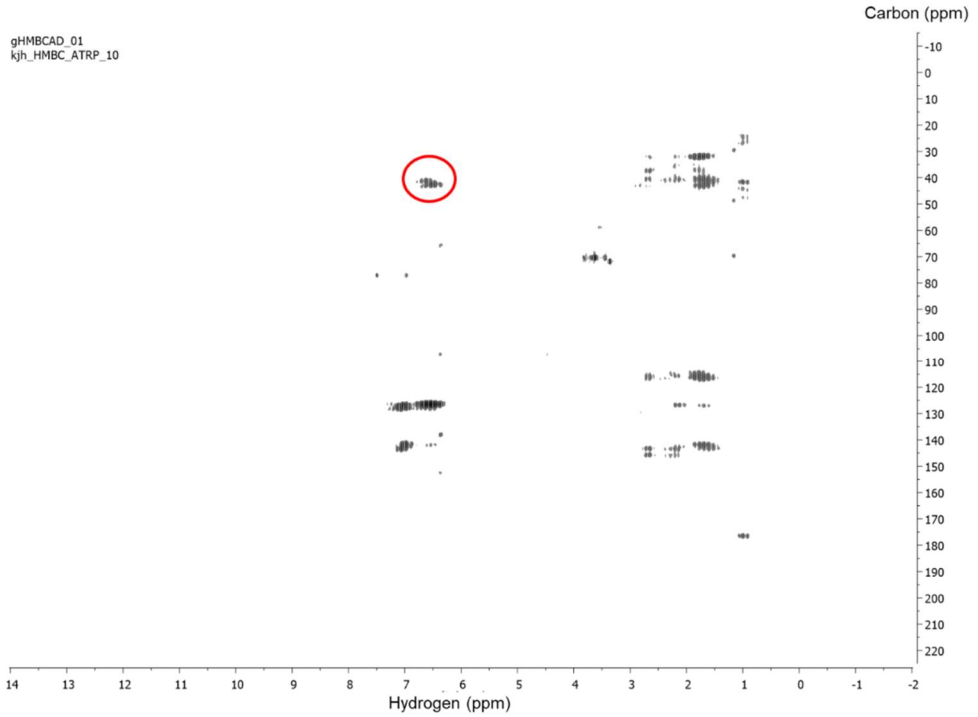

Fig. 12 Entire image of ^{1}H-^{13}C heteronuclear multiple bond correlation (HMBC) data and red circle is enlarged image represented in Fig. 2B

Post polymerization modification – Azide substitution on the para position of 2,3,4,5,6-pentafluorostyrene group.

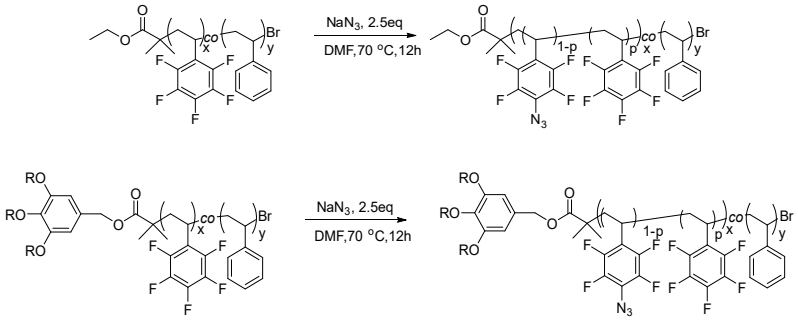

Scheme 4. Preparation of azide-substituted P(pFS-*co*-Sty) and $(PEG550)_3$-P(pFS-*co*-Sty)

P(pFS-*co*-Sty) (520 mg) and sodium azide (NaN_3) (0.6 g, 5 equiv. of 2,3,4,5,6-pentafluorostyrene groups) were dissolved in DMF (6 mL) and stirred at preheated oil bath (70 °C) for overnight. Then, the solution was precipitated in stirring methanol (50 mL). A yellowish white powder P(pFS-*co*-Sty)-N_3 (520 mg) was collected by vacuum filtration and dried. The molecular weight and composition of the polymers were characterized by ^{1}H NMR, ^{19}F NMR and FT-IR.

Self-assembly of block copolymers and photo-crosslinking of self-assembled structures.

The prepared polymer (10 mg) was dissolved in 1,4-dioxane or THF (2 mL) in a 20 mL capped vial with a magnetic bar. The solution was stirred for 1 h at room temperature (800 rpm). A syringe pump was calibrated to deliver water at a speed of 0.5 mL h^{-1}. The vial cap was replaced by a rubber septum and water was added to the polymer solution for 4 h using a syringe pump with a 6-mL syringe equipped with a steel needle. The resulting suspension was subjected to dialysis (molecular weight cutoff ~12 to 14 kDA (SpectraPor)) against water for 72 h (with frequent changes). The dialyzed suspension (1 mL) was transferred to 4-mL capped vial with a magnetic bar. The solution (1 mL, 1 mg mL^{-1}) containing the self-assembled structure of BCPs in a 3 mL of vial was exposed to short-wavelength UV light (λ = ~280 nm, 20 W) for 8 h with air-blowing (for temperature control) located 1 cm away from the vial. After 8 h, the solution was transferred to the mixture (H_2O : THF = 1 to 10 ratio) to test the physical stability of the cross-linked nanoparticles in chemically harsh condition.

Synthesis of proline with alkyne linker (p-alkyne).

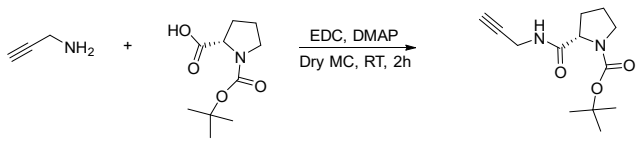

Scheme 5. Synthetic scheme of tert-butyl (S)-2-(prop-2-yn-1-ylcarbamoyl)pyrrolidine-1-carboxylate.

N-(tert-Butoxycarbonyl)-L-proline (4.3 g, 20 mmol), propargylamine (1.32 g, 1.54 ml, 24 mmol) 4-Dimethylaminopyridine (367 mg, 3 mmol) were dissolved in dry CH_2Cl_2 (100 mL) in a Schlenk flask (250 mL) and stirred under 0°C condition. 1-Ethyl-3-(3-dimethylaminopropyl) carbodiimide (4.98 g, 26 mmol) dissolved in dry CH_2Cl_2 (25 mL) was transferred to first solution mixture with cannula. After 15 h, reaction was quenched by adding water (50 mL) and product extracted with CH_2Cl_2 (50 mL × 3 times). The collected organic phases were dried over $MgSO_4$, and evaporated under reduced pressure. The mixture was purified by column chromatography with mixture of hexane and EA (1:1). The first fraction was collected and dried at a reduced pressure. Recrystallization in hexane at 20 ˚C to afford the white solid.[1] The molecule is characterized with ^{1}H NMR and ^{13}C NMR. δH ($CDCl_3$) 7.26 and 6.27 (s, 0.5H and s, 0.5H, NH), 4.24 (m, 1H, CH), 3.98 (m, 2H, $CH_2C\equiv$), 3.43 (m, 2H, CH_2N), 2.21 (m, 1H, C*H*HCHN), 2.19 (s, 1H, HC$\equiv$), 1.85 (br s, 3H, CH*H*CHN, C*H*$_2$CH$_2$CHN), 1.44 (m, 9H, $(CH_3)_3$); δC ($CDCl_3$) 172.42 and 171.85 (*C*ONHCH$_2$), 156.12 and 154.73 (CO Boc), 80.84 (*C*$(CH_3)_3$), 79.59 (HC$\equiv$), 71.85 and 71.42 (*C*$\equiv$CH), 61.25 and 59.89 (CHN), 47.22 (CH_2N), 31.05 and 27.94 (*C*H$_2$CHN), 29.14 (*C*H2C$\equiv$), 28.46 (C(*C*H$_3$)$_3$), 23.93 and 24.68 (*C*H$_2$CH$_2$N).

Basic analysis of polymer material's physical property

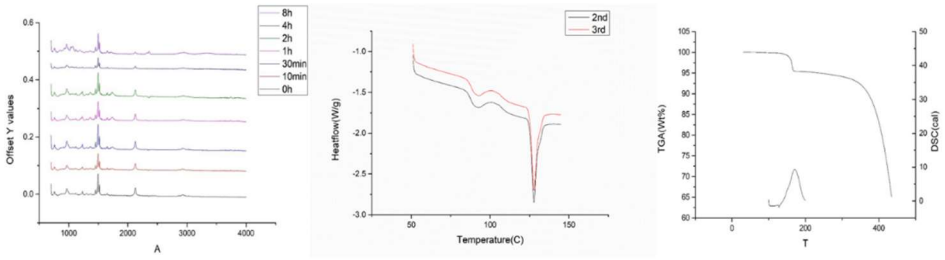

Fig. 13 (A) FT-IR spectra of **H1** in THF (0.01 mg mL^{-1}) with irradiation of short-wavelength UV light (λ = 280 nm) for increasing exposure times. (B) Differential scanning calorimetry (DSC) and (C) Thermo Gravimetric Analysis (TGA) spectra of **H1** and **H1-** N_3.

After azide modification of **H1**, DSC and TGA both showed thermal degradation of pendant azide group in pentafluorostyrene moiety. The photo-degradation of the azide pendant groups of the polymer chains under UV irradiation (= ~280nm) was studied in solution. The photo-degradation of the pendant azide groups of P(pFS-*co*-Sty) (**H1-** N_3) in THF (0.01 mg mL^{-1}) was observed by IR spectroscopy after UV light irradiation (λ = ~280 nm, 20 W). There was a sequential decrease of the azide peaks in IR spectrum that degradation of N≡N bond expose under the UV light (λ = ~280 nm, 20 W) (Fig. S5A). We also investigated the thermal property of **H1** before and after azide substitution. Differential scanning calorimetry (DSC) of **H1** before azidification showed the glass transition temperature (T_g) at 89 °C with the sharp endothermic peak at 125 °C. The result was explained with π-π stacking between styrene group and 2,3,4,5,6-pentaflurorostyrene group (Fig. S5B).[2] After azide modification, DSC and Thermo Gravimetric Analysis (TGA) both showed thermal degradation of pendant azide group in pentafluorostyrene moiety (Fig. S5C).[3]

Synthesis of telechelic functionalized linear block copolymer with click reaction & TMS deprotection of linear polymer and CuAAC reaction between bis-azide (PEG2000).

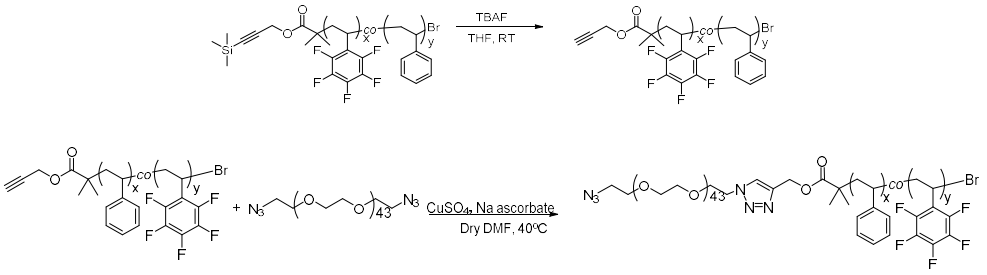

Scheme 6. (A) TMS deprotection of TMS-alkyne-P(pFS-*co*-Sty). (B) Coupling of bis-azide PEG and alkyne-P(pFS-*co*-Sty) via CuAAC reaction.

The TMS-alkyne-P(pFS-*co*-Sty) solution in THF (5 mL) was prepared in a 20 mL glass vial and excess amount of tetra-*n*-butyl ammonium fluoride (TBAF) added into the TMS-alkyne-P(pFS-*co*-Sty) solution and stirred for 5 h at room temperature. After the reaction completed, the alkyne-P(pFS-*co*-Sty) solution with TBAF precipitated in MeOH (50 mL). The white powder was collected by vacuum filtration and dried. For the click reaction, $CuSO_4$ (40 mg) and Sodium ascorbate (30 mg) was completely dried in vacuum for 15 min. Dry DMF (1.5 mL) was added into the vial. The resulting mixture was stirred under N_2 condition for 15 min. To this solution, a solution of the hydrophilic bis-azide (PEG2000) block and collected alkyne-P(pFS-*co*-Sty) hydrophobic part polymer (10 eq. to the hydrophilic module) in DMF (5 mL) was added into the prepared solution containing the reagents of click reaction. The mixture was degassed by bubbling N_2 gas for 15 min. After degassing, the click reaction was proceeded at 40 °C until reaction completion. The extent of the reaction was monitored by GPC. The reaction

was quenched by exposing the solution to air, followed by dilution with chloroform. The cooled solution was filtered through aluminum oxide (basic) with $CHCl_3$ to remove the Cu catalyst. The filtered solution was precipitated in cold MeOH (50 mL) to afford white powdery product. If necessary, the resulting block copolymer was purified by preparatory size exclusion chromatography.

CuAAC reaction between alkyne terminal boc-protected proline group, followed by boc deprotection for activating functional group in the telechelic part of the polymer.

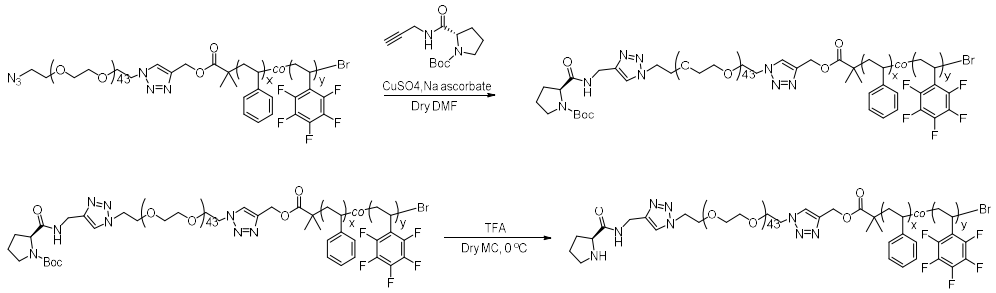

Scheme 7. (A) CuAAC reaction between azide-(PEG2000)-P(pFS-*co*-Sty) and boc protected L-proline-alkyne. (B) Boc deprotection of proline telechelic block copolymer.

For the click reaction, $CuSO_4$ (40 mg) and Sodium ascorbate (30 mg) was completely dried in vacuum for 15 min. Dry DMF (1.5 mL) was added into the vial. The resulting mixture was stirred under N_2 condition for 15 min. To this solution, a solution of the (S)-2-(prop-2-yn-1-ylcarbamoyl) pyrrolidine-1-carboxylate and collected azide-(PEG2000)-P(pFS-*co*-Sty) amphiphilic block copolymer (10 eq. to the boc-protected catalyst module) in DMF (5 mL) was added into the prepared solution containing the reagents of click

reaction. The mixture was degassed by bubbling N_2 gas for 15 min. After degassing, the click reaction was proceeded at 40 °C until reaction completion. The extent of the reaction was monitored by GPC. The reaction was quenched by exposing the solution to air, followed by dilution with chloroform. The cooled solution was filtered through aluminum oxide (basic) with $CHCl_3$ to remove the Cu catalyst. The filtered solution was precipitated in cold MeOH (50 mL) to afford white powdery product. The boc-proline-(PEG2000)-P(pFS-*co*-Sty) solution in CH_2Cl_2 (2 mL) was prepared in a 20 mL glass vial trifluoroacetic acid (TFA, 1 mL) added in to the boc-proline-(PEG2000)-P(pFS-*co*-Sty) solution and stirred for 2 hr in 0 °C condition. After 2 hours, proline-(PEG2000)-P(pFS-*co*-Sty) solution with TFA precipitated in MeOH (50 ml). The white powder was collected by vacuum filtration.

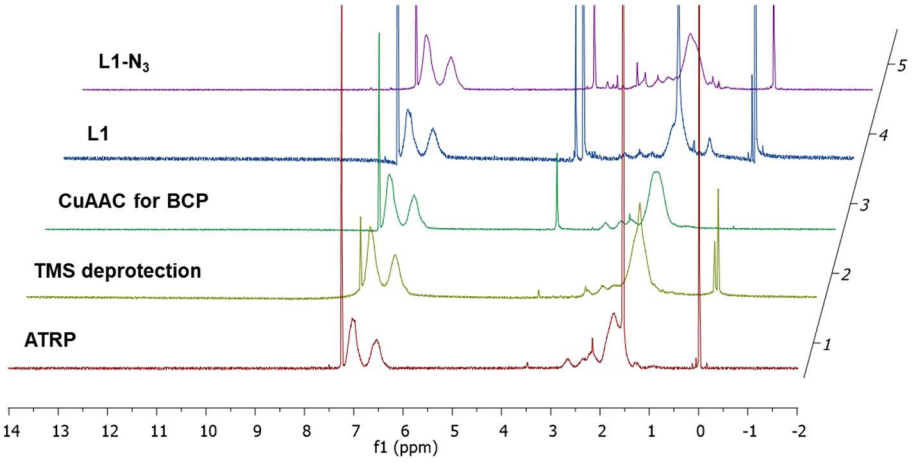

Fig. 14 Entire ^{1}H-NMR data of L1-N_3 resulting polymer and their intermediates.

Photo-crosslinking of the self-assembled structures of BCPs

Self-assembly of block copolymers and photo-crosslinking of self-assembled structures.

The prepared polymer (10 mg) was dissolved in 1,4-dioxane or THF (2 mL) in a 20 mL capped vial with a magnetic bar. The solution was stirred for 1 h at room temperature (800 rpm). A syringe pump was calibrated to deliver water at a speed of 0.5 mL h^{-1}. The vial cap was replaced by a rubber septum and water was added to the polymer solution for 4 h using a syringe pump with a 6-mL syringe equipped with a steel needle. The resulting suspension was subjected to dialysis (molecular weight cutoff ~12 to 14 kDA (SpectraPor)) against water for 72 h (with frequent changes). The dialyzed suspension (1 mL) was transferred to 4-mL capped vial with a magnetic bar.

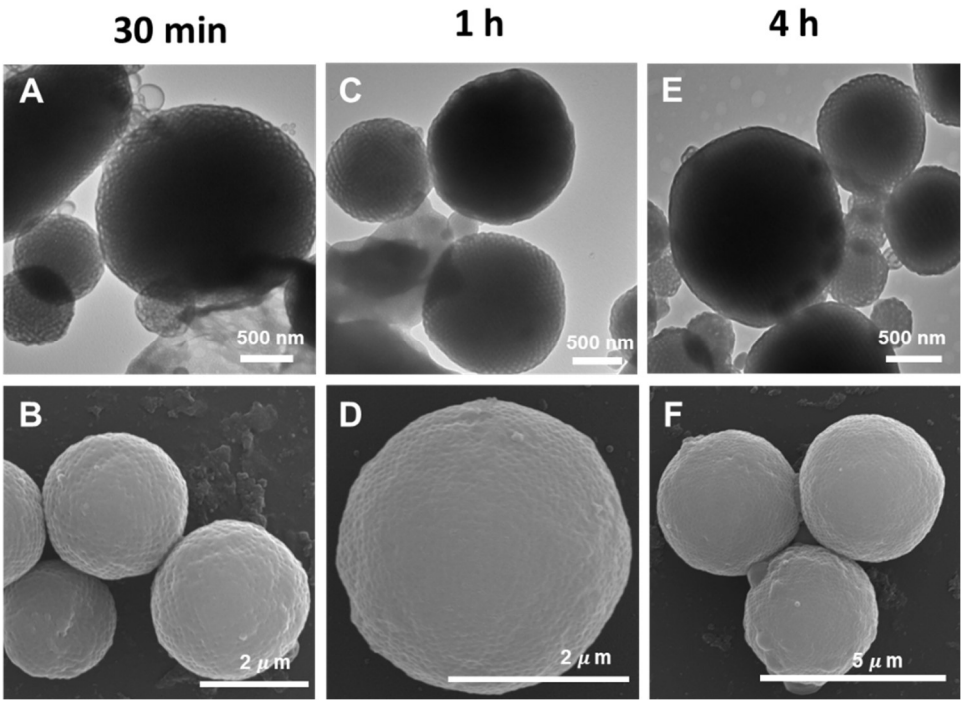

Fig. 15 (A, C and E) TEM and (B, D and F) SEM images of the self-assembled and inner structure of **BCP1** as a function of the water-injection time: (Time of water

addition (t) = 30 min for A and B) polymer cubosomes; (t = 1 h for C and D) polymer cubosomes ; and (t = 4 h for E and F) polymer cubosomes

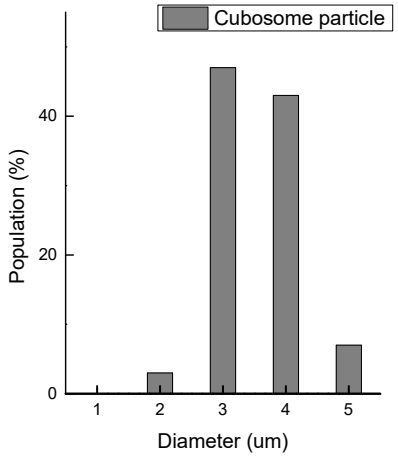

Fig. 16 Average size (3.03μm) and distribution of the polymer cubosome particles. The particle size distribution of polymer cubosomes was measured by analyzing SEM images of polymer cubosomes with ImageJ software. 50 particles were selected for the image analysis from SEM images taken from 5-10 different positions.

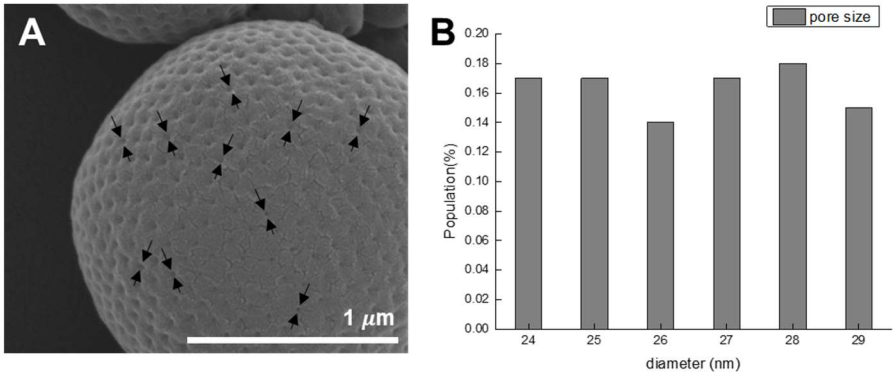

Fig. 17 The average pore size at the circumference of polymer cubosomes was determined by analyzing SEM images of polymer cubosomes with ImageJ software. 10 pores were selected for the image analysis from SEM images taken from 10 different particles. (A) Example of selected pore in cubosome particle (B) Distribution of the pore size.

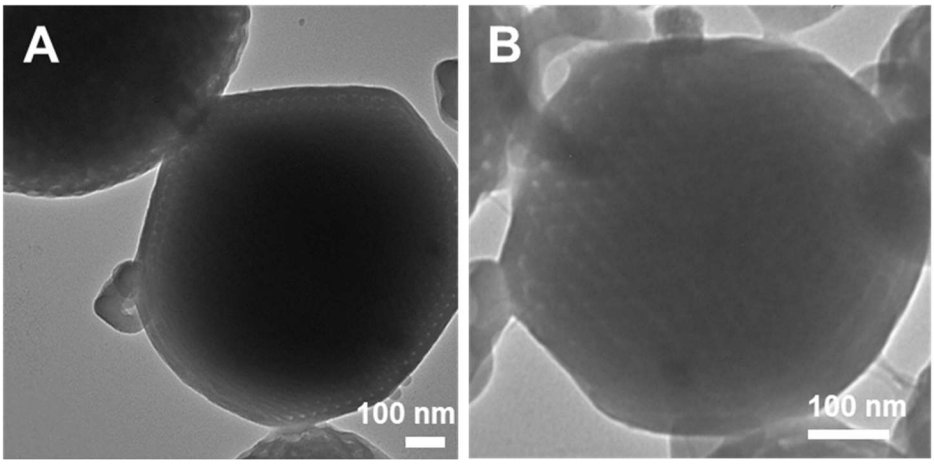

Fig. 18 TEM image of the photo-crosslinked polymer cubosome sustain their complex inner structure in organic solvent (A) DMSO, (B) Dioxane.

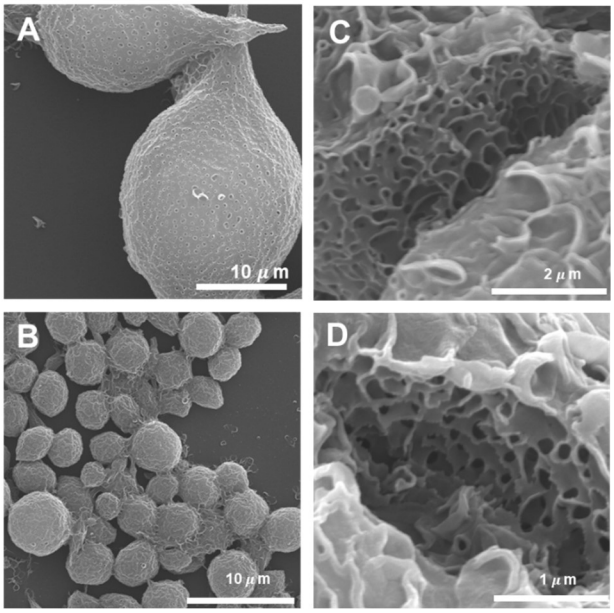

Fig. 19 (A, B, C and D) SEM images of the self-assembled and inner structure of **BCP2** as a function of the water-injection time: (Time of water addition (t) = 1 h for A and C) fibroblast shaped sponge phase particles and inner structure; (t = 30 min for B and D) Spherical shaped sponge phase particles and inner structure.

Photo-crosslinking of self-assembled structure.

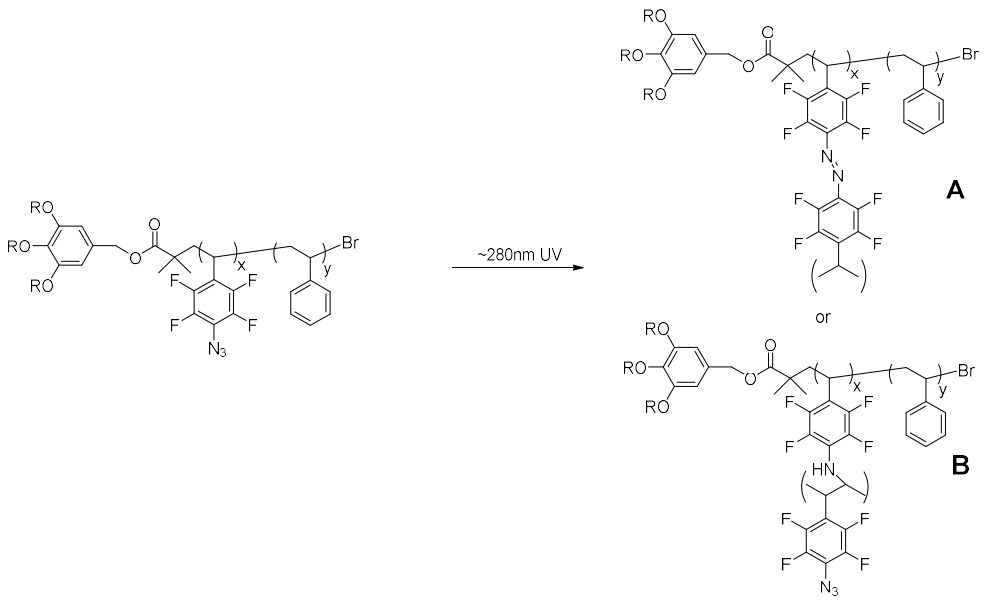

Scheme 8. Scheme of photo-crosslinking between hydrophobic blocks of the **BCP1-**N_3 under UV (~280 nm) irradiation.

The solution (1 mL, 1 mg mL^{-1}) containing the self-assembled structure of BCPs in a 3 mL of vial was exposed to short-wavelength UV light (λ = ~280 nm, 20 W) for 8 h with air-blowing (for temperature control) located 1 cm away from the vial. After 8 h, the solution was transferred to the mixture (H_2O : THF = 1 to 10 ratio) to test the physical stability of the cross-linked nanoparticles in chemically harsh condition.

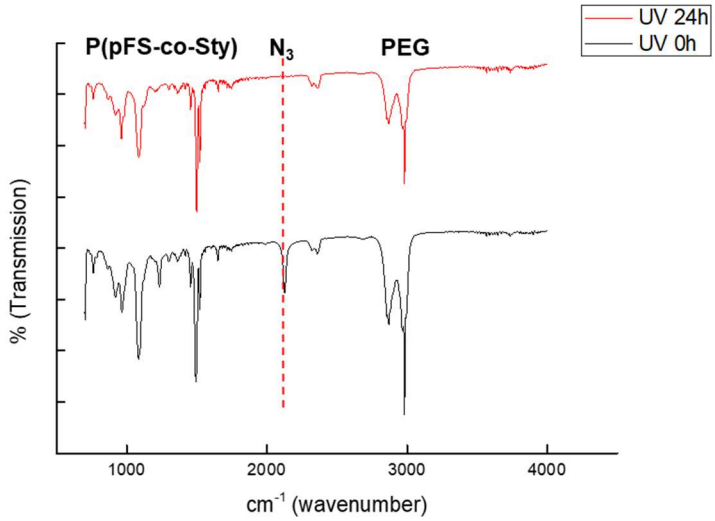

Fig. 20 FT-IR spectra of the self-assembled polymer cubosome before UV irradiation (black), after UV irradiation 24h (red).

Asymmetric aldol reaction on cubosome reactor and chiral stationary phase HPLC

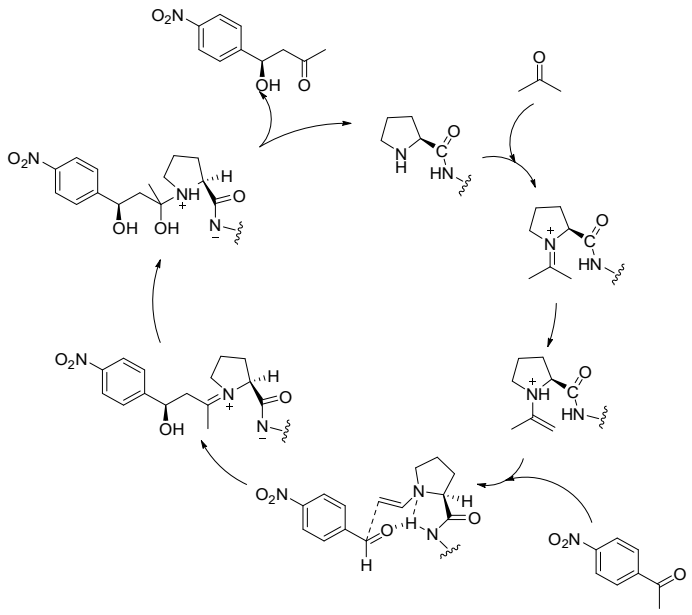

Scheme 9. Catalytic cycle for asymmetric aldol reaction in the presence of telechelic L-proline.

Asymmetric aldol reaction with proline-tethered cubosome based structure.

The cross-linked polymer cubosomes of **BCP1-** N_3/ **L1-** N_3 (9:1) (50 mg) in the mixture of THF (1.8 mL) and water (0.2 mL) was prepared in a capped vial, followed by addition of 4-Nitrobenzaldehyde (3.6 mg, 15 μmol) and acetone (200 μL) in the vial. After the reaction was stirred for 72 h, the mixture was quenched by adding saturated NH_4Cl solution and polymer particles were separated from solution by centrifuge (14,000 rpm, 10 min). The product in supernatant was extracted with CH_2Cl_2 (1 mL × 3 times), dried over $MgSO_4$, and evaporated under reduced pressure. The collected polymer cubosome particles are redispersed in the same solution condition (THF (1.8 mL) and water (0.2 mL). The asymmetric aldol reaction were repeatedly proceeded to perform the reusability test (6 times).

Comparing reaction conversion rate between proline functionalized cubosome based structure and L-proline in homogeneous state.

The amount of L-proline (15 μg, 0.13 μmol) was calculated by molecular amount of **L1-**N_3 (M_w = 41k g mol^{-1}, insertion weight 5 mg in polymer cubosome 50 mg). To the mixture of THF (1 mL) and water (1 mL) (to prevent proline solubility issue), 4-Nitrobenzaldehyde (3.6 mg, 15 μmol) and acetone (200 μL) were added. During the reaction, a small amount of mixture was extracted and quenched by

adding saturated NH_4Cl solution and the reaction mixture in solution extracted with CH_2Cl_2 (1 mL × 3 times). The organic phases were collected, dried over $MgSO_4$, and evaporated under reduced pressure. For comparative group, The **BCP1-** N_3**/L1-** N_3 (9:1) polymer cubosome (50 mg) solution in THF (1 mL) and water (1 mL), was prepared in a capped vial and mixed with 4-Nitrobenzaldehyde (3.6 mg, 15 μmol) and acetone (200 μL) for 72 h with stirring. During the reaction, a small amount of mixture was extracted and quenched by adding saturated NH_4Cl solution and polymer particles were separated from solution by centrifuge (14,000 rpm, 10 min). The product in supernatant was extracted with CH_2Cl_2 (1 mL × 3 times), dried over $MgSO_4$, and evaporated under reduced pressure.

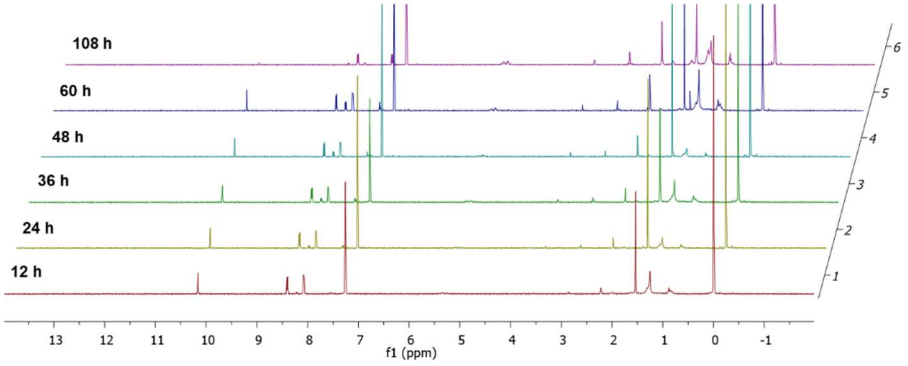

Fig. 21 ^{1}H-NMR result by time for the percentage conversion of the asymmetric aldol reaction by homogeneous proline.

Chiral stationary phase HPLC methods condition.

Reagents: Hexane (gradient HPLC grade from Honeywell (Art. No.65801)), IrOH (gradient grade from J.T. Baker (Art. No.65702)). Sample solvent: MeOH, 2.0 mg mL^{-1}, injection volume: 5 μL, column: Chiralpak IA, 250 x 4.6 mm, 5 μm (Daicel), flow rate: 1 mL/min, run time: 30.0 min, column temperature: 30 °C, detection

(DAD) at 254 nm (BW16nm), mobile phase: hexane/IrOH (9:1). Retention time of the minor/major products are 13.95 min/14.17 min and % ee of products are 44%.

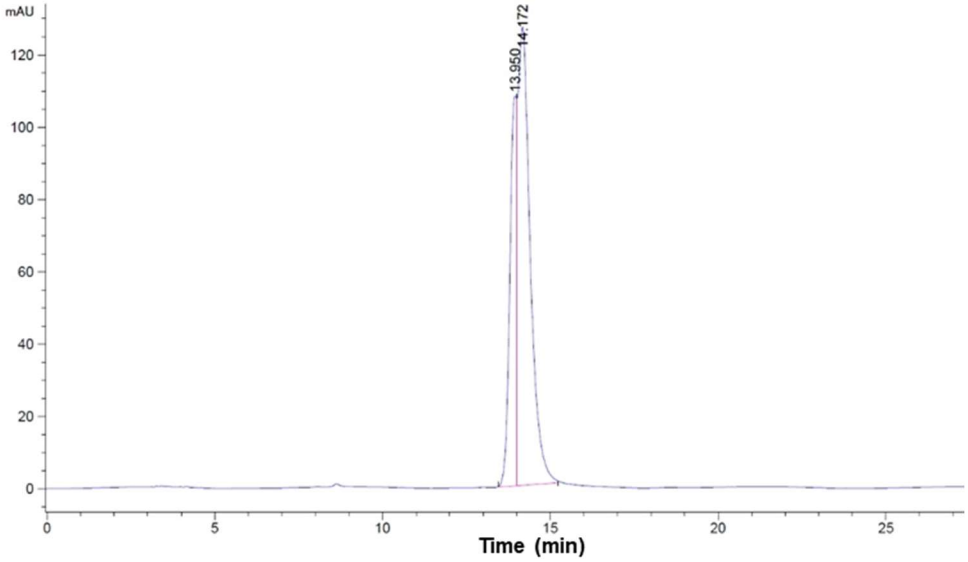

Fig. 22 Chiral HPLC result of product (R)-4-hydroxy-4-(4-nitrophenyl) butan-2-one.

REFERENCES

(1) X. Wang, J. Feng, Y. Bai, Q. Zhang, Y. Yin, *Chem. Rev.,* 2016, **116**, 10983–11060.

(2) C. G. Palivan, O. Fischer-Onaca, M. Delcea, F. Itel, W. Meier, *Chem. Soc. Rev.,* 2012, **41**, 2800–2823.

(3) M. Vázquez-González, C. Wang, I. Willner, *Nat. Catal.,* 2020, **3**, 256–273.

(4) C. LoPresti, H. Lomas, M. Massignani, T. Smart, G. Battaglia, *J. Mater. Chem.,* 2009, **19**, 3557–3776.

(5) M. Marguet, C. Bonduelle, S. Lecommandoux, *Chem. Soc. Rev.,* 2013, **42**, 512–529.

(6) J. Gaitzsch, X. Huang, B. Voit, *Chem. Rev.,* 2016, **116**, 1053–1093.

(7) H. Che, S. Cao, J. C. M. van Hest, *J. Am. Chem. Soc.,* 2018, **140**, 5356–5359.

(8) K. T. Kim, S. A. Meeuwissen, R. J. Nolte, J.C. M. van Hest, *Nanoscale,* 2010, **2**, 844–858.

(9) N. E. Leadbeater and M. Marco, *Chem. Rev.*, 2002, **102**, 3217-3273.

(10) A. Lu and R. K. O'Reilly, *Curr. Opin. Biotechnol.*, 2013, **24**, 639–645.

(11) C. T. Womble, M. Kuepfert, A. E. Cohen and M. Weck, *Macromol. Rapid Commun.*, 2019, **40**, 1800580.

(12) S. Ha, Y. La, K. T. Kim, *Acc. Chem. Res.,* 2020, **53**, 620.

(13) Y. La, C. Park, T. J. Shin, S. H. Joo, S. Kang, K. T. Kim, *Nat. Chem*., 2014, **6**, 534−541.

(14) S. J. Holder, N. A. J. M. Sommerdijk, *Polym. Chem.,* 2011, **2**, 1018−1028.

(15) H. Yu, X. Qiu, S. P. Nunes, K.-V. Peinemann, *Nat. Commun*., 2014, **5**, 4110.

(16) X. Lyu, A. Xiao, W. Zhang, P. Hou, K. Gu, Z. Tang, H. Pan, F. Wu, Z. Shen, X.-H. Fan, *Angew. Chem., Int. Ed.,* 2018, **57**, 10132−10136.

(17) Y. La, T. H. An, T. J. Shin, C. Park, K. T. Kim, *Angew. Chem., Int. Ed.,* 2015, **54**, 10483–10487.

(18) H. Liu, L. Ren, H. Wu, Y.-L. Ma, S. Richter, M. Godehardt, C. Kübel, W. Wang, *J. Am. Chem. Soc*., 2019, **141***,* 831–839.

(19) L. Han, S. Che, *Adv. Mater*., 2018, **30**, 1705708.

(20) Z. Lin, S. Liu, W. Mao, H. Tian, N. Wang, N. Zhang, F. Tian, L. Han, X. Feng, Y. Mai, *Angew. Chem., Int. Ed*., 2017, **56**, 7135−7140.

(21) S. Bobbala, S. D. Allen, E. A. Scott, *Nanoscale,* 2018, **10**, 5078−5088.

(22) J. Wang, Q. Ma, Y. Wang, Z. Li, Z. Li, Q. Yuan, *Chem. Soc. Rev.,* 2018, **47**, 8766–8803.

(23) Y. La, J. Song, M. G. Jeong, A. Cho, S.-M. Jin, E. Lee, K. T. Kim, *Nat. Commun*., 2018, **9**, 5327.

(24) Z. Lin, J. Zhou, C. Cortez-jugo, Y. Han, Y. Ma, S. Pan, E. Hanssen, J. J. Richardson, F. Caruso, *J. Am. Chem. Soc*., 2020, **142**, 335–341.

(25) H. Lee, D. Kim, H. Ma, K. T. Kim, *Chem. Commun*., 2020, **56**, 14059–14062.

(26) T. H. An, Y. La, A. Cho, M. G. Jeong, T. J. Shin, C. Park, K. T. Kim, *ACS Nano,* 2015, **9**, 3084−3096.

(27) S. D. Allen, S. Bobbala, N. B. Karabin, E. A. Scott, *Nanoscale Horiz*., 2019, **4**, 258−272.

(28) M. Duss, L. Salvati Manni, L. Moser, S. Handschin, R. Mezzenga, H. J. Jessen, E. M. Landau, *ACS Appl. Mater. Interfaces,* 2018, **10**, 5114−5124.

(29) S. T. Hyde, *J. Phys. Chem.,* 1989, **93**, 1458–1464.

(30) R. H. Templer, J. M. Seddon, P. M. Duesing, R. Winter, J. Erbes, *J. Phys. Chem. B,* 1998, **102**, 7262–7271.

(31) H. M. G. Barriga, M. N. Holme, M. M. Stevens, *Angew. Chem., Int. Ed.,* 2019, **58**, 2958–2978.

(32) R. Mezzenga, J. M. Seddon, C. J. Drummond, B. J. Boyd, G. E. Schröder-Turk, L. Sagalowicz, *Adv. Mater.,* 2019, **31**, 1900818.

(33) M. Duss, J. J. Vallooran, L. S. Manni, N. Kieliger, S. Handschin, R. Mezzenga, H. J. Jessen, E. M. Landau. *Langmuir,* 2019, **35**, 120-127.

(34) B. M. Discher, H. Bermudez, D. A. Hammer, D. E. Discher, Y.-y.Won, F. S. Bates, *J. Phys. Chem. B,* 2002, **106**, 2848−2854.

(35) D. Yang, D. O'Brien, S. Marder, *J. Am. Chem. Soc.,* 2002, **124**, 13388–13389.

(36) M. G. Jeong, K. T. Kim, *Macromolecules,* 2017, **50**, 223−234.

(37) J. Kim, M. Yoon, S.-M. Jin, J. Lee, Y. La, E. Lee, K. T. Kim, *Polym. Chem*., 2019, **10**, 3778−3785.

(38) H. Wang, P. B. Zetterlund, C. Boyer, P. T. Spicer, *J. Colloid Interface Sci*., 2019, **546**, 240−250.

(39) M. Albuszis, P. J. Roth, W. Pauer, H.-U. Moritz, *Polym. Chem*., 2016*,* **7**, 5414–5425.

(40) K. L. Buchmueller, B. T. Hill, M. S. Platz, K. M. Weeks, *J. Am, Chem. Soc*., 2003, **125**, 10850–10861.

(41) J.-M. Noy, Y. Li, W. Smolan, P. J. Roth, *Macromolecules,* 2019, **52**, 3083–3091.

(42) J. Chen, L. Dumas, J. Duchet-Rumeau, E. Fleury, A. Charlot, D. Portinha, *J. Polym. Sci., Part A: Polym. Chem.,* 2012, **50**, 3452−3460.

(43) J. F. W. Keana, S. X. Cai, *J. Org. Chem*., 1990, **55**, 3640–3647.

(44) K. Jankova, S. Hvilsted, *Macromolecules,* 2003, **36**, 1753–1758.

(45) J. D. Zeng, J. Zhu, X. Q. Pan, Z. B. Zhang, N. C. Zhou, Z. P. Cheng, W. Zhang, X. L. Zhu, *Polym. Chem*., 2013*,* **4**, 3453−3457.

(46) S. Nishimura, A. Nagai, A. Takahasmi, T. Narita, T. Hagiwara, H. Hamana, *Polym. J*., 1990, **22**, 171−174.

(47) C. Pugh, C. N. Tang, M. Paz-Pazos, O. Samtan, A. H. Dao, *Macromolecules,* 2007, **40**, 8178−8188.

(48) F. Lv, Z. An, P. Wu, *Nat. Commun*., 2019, **10**, 1397−1403.

(49) N. ten Brummelhuis, M. Weck, *ACS Macro Lett*., 2012, **1**, 1216−1218.

(50) J.-P. O'Shea, V. Solovyeva, X. Guo, J. Zhao, N. Hadjichristidis, V. O. Rodionov, *Polym. Chem*., 2014, **5**, 698−701.

(51) L. Sagalowicz, M. Michel, M. Adrian, P. Frossard, M. Rouvet, H. J. Watzke, A. Yaghmur, L. De Campo, O. Glatter, M. E. Leser, *J. Microsc.,* 2006, **221**, 110–121.

(52) B. List, R. A. Lerner, C. F. Barbas, *J. Am. Chem. Soc.,* 2000, **122**, 2395–2396.

(53) S. Chandrasekhar, N. R. Reddy, S. S. Sultana, C. Narsihmulu, K. V. Reddy, *Tetrahedron,* 2006, **62**, 338–345.

국문초록

유기 용매에서 재활용 가능한 나노반응기로서의 광-가교 되어진 고분자 큐보좀에 대한 연구

고분자 큐보좀은 고도의 비대칭 블록 비율을 갖는 블록 공중합체의 수용액상 자기조립에 의해 형성되는 복잡한 구조의 다공성 구조이다. 이러한 고분자 큐보좀이 가진 내부 나노 채널 네트워크는 촉매를 수용할 수 있는 큰 표면적과 내부 체적을 제공하는 망상 다공성 구조를 가진 나노 반응기의 유망한 후보로 볼 수 있다.

당해 연구에서는 폴리 (에틸렌 글리콜)의 친수성 부분 및 폴리 (스타이렌 -공- 펜타 플루오로스타이렌)의 소수성 블록으로 구성된 양쪽성 블록 공중합체를 합성하였다. 소수성 블록의 펜타 플루오로 페닐기는 중합 후 간단한 반응에 의해 아자이드 반응기로 쉽게 광-가교 가능하도록 기능화 하기 위해 도입되어졌으며, 분기 선형 및 촉매 기능화된 선형 블록 공중합체로 구성된 두 성분 혼합물은 수용액상에서의 자기 조립을 거쳐 표면에 촉매가 심어진 고분자 큐보좀의 형태로 만들어졌고, 해당 구조는 자외선의 조사로 얻어낸 광-가교 반응을 활용하여 유기 용매와 같은 극한 환경에서도 복잡한 내부 형태를 유지 하는 것을 관찰 하였다. 이렇게 얻어진 고분자 큐보좀 나노 반응기는 표면에 심어진 유기 촉매에 의해 유기 용매 중에서 4- 니트로 벤즈알데히드와 아세톤의 비대칭 알돌 반응을 촉진하여 (R) -4- 히드록시 -4- (4- 니트로 페닐) 부탄 -2- 온을 더 높은 속도로 생성할 수 있음을 확인하였다. 이에 더하여 해당 나노 반응기가 여러 번의 재활용 과정 에서도 촉매 효율과 구조적 복잡성을 잃지 않고 반복 촉매 작용을 수행하는 것을 보였다.

주요어 : 블록 공중합체, 광-가교, 유기 촉매 반응, 수용액 상 자기조립, 큐보좀

학 번 : 2019-27820